Functionalized PCL/HA nanocomposites as microporous membranes for bone regeneration

Maria Assunta Bassile, Giovanna Gomez D'ayala, Mario Malinconico, Paola Laurienzo, Jean Coudane, Benjamin Nottelet, Fulvio Della Ragione, Adriana Oliva

Functionalized PCL/HA nanocomposites as microporous membranes for bone regeneration

Maria Assunta Basile [a], Giovanna Gomez d'Ayala [a], Mario Malinconico [a], Paola Laurienzo [a,*], Jean Coudane [b], Benjamin Nottelet [b], Fulvio Della Ragione [c], Adriana Oliva [c,*]

[a] Institute for Polymers, Composites and Biomaterials, CNR, Via Campi Flegrei 34, Pozzuoli (Naples), Italy
[b] Institut des Biomolécules Max Mousseron (IBMM), Artificial Biopolymers Group, CNRS UMR 5247, University of Montpellier 1, Faculty of Pharmacy, 15 Av. C. Flahault, Montpellier 34093, France
[c] Department of Biochemistry and Biophysics, Second University of Naples, Via L. De Crecchio 7, Naples, Italy

Keywords:
Poly(ε-caprolactone)
Functionalization of polymers
Nanocomposites
Membranes
Biocompatibility
Guided tissue regeneration

A B S T R A C T

In the present work, microporous membranes based on poly(ε-caprolactone) (PCL) and PCL functionalized with amine (PCL-DMAEA) or anhydride groups (PCL-MAGMA) were realized by solvent–non solvent phase inversion and proposed for use in Guided Tissue Regeneration (GTR). Nanowhiskers of hydroxyapatite (HA) were also incorporated in the polymer matrix to realize nanocomposite membranes. Scanning Electron Microscopy (SEM) showed improved interfacial adhesion with HA for functionalized polymers, and highlighted substantial differences in the porosity. A relationship between the developed porous structure of the membrane and the chemical nature of grafted groups was proposed. Compared to virgin PCL, hydrophilicity increases for functionalized PCL, while the addition of HA influences significantly the hydrophilic characteristics only in the case of virgin polymer. A significant increase of in vitro degradation rate was found for PCL-MAGMA based membranes, and at lower extent of PCL-DMAEA membranes. The novel materials were investigated regarding their potential as support for cell growth in bone repair using multipotent mesenchymal stromal cells (MSC) as a model. MSC plated onto the various membranes were analyzed in terms of adhesion, proliferation and osteogenic capacity that resulted to be related to chemical as well as porous structure. In particular, PCL-DMAEA and the relative nanocomposite membranes are the most promising in terms of cell-biomaterial interactions.

1. Introduction

Poly(ε-caprolactone) (PCL) is a synthetic polyester with high biocompatibility and slow in vivo degradation rate, thus providing an adequate support until regeneration is completed [1]. Low resorption rate recommends PCL for long-term applications, as slow release of bioactive molecules and extended-residence cell supports in tissue engineering, while its good flexibility makes it an interesting candidate in the area of guided tissue regeneration (GTR) as membrane for the treatment of periodontal diseases [2–4]. Membranes for use in GTR are required to be degradable, with degradation time adequate to bone regeneration, to prevent migration of gingival epithelial cells into the alveolar cavity delaying bone formation, to accelerate cementogenesis, and to protect the site from the underlying blood clots, so allowing healing process. Combination of membranes with growth factors or osteoconductive calcium phosphates to allow better bone formation is expected to improve the overall performance. In this regard, PCL nanocomposites with hydroxyapatite (HA), the natural occurring mineral phase of bone [5–10], can be of interest. Bone is a true nanocomposite consisting of nanocrystalline HA dispersed in a collagen-rich matrix. Nanocrystalline HA promotes osteoblast cell adhesion, differentiation and proliferation better than microcrystalline HA [11,12]. As an added value, whisker-like nanocrystals (nanowhiskers) are considered to improve toughness and promote cell alignment in bioceramics and PCL nanocomposites [13]. A major limit of PCL/HA nanocomposites is represented by the strong hydrophobic character of PCL that inhibits realization of composites with good dispersion and interfacial adhesion of the two phases. A good interface is fundamental to improve mechanical characteristics of the polymer matrix, and interfacial phenomena may also play a role in cellular response [14,15]. In this frame, functionalization is a particularly relevant approach in order to broadly change the physicochemical properties of a polymer in a tailored way by selective chemical modification. Functionalization under controlled conditions may increase degradation rate by reducing crystallinity, creating interchain hydrogen bondings to modulate mechanical properties, and improving adhesion with hydrophilic fillers.

In a previous work [16], we studied the biological characteristics of two different functionalized PCLs, and found that PCLs modified by grafting of N-dimethylamino-ethyl acrylate (PCL-DMAEA) or maleic anhydride/glycidyl methacrylate (PCL-MAGMA) showed differences in

* Corresponding authors.
E-mail addresses: paola.laurienzo@ipcb.cnr.it (P. Laurienzo), adriana.oliva@unina2.it (A. Oliva).

biocompatibility and cell adhesion with respect to pristine polymer. Related HA nanocomposites, with HA in form of nanowhiskers, were also evaluated, and a better interfacial adhesion between polymer matrix and HA was found in the case of functionalized PCL. In the present paper, PCL, functionalized PCL and relative HA nanocomposites were prepared in the form of microporous membranes for application in GTR. A solvent–non solvent phase inversion technique was used. Previous studies have shown that this methodology allows to obtain membranes with a gradational changed porosity as a function of polymer solution concentration [17], or through an appropriate choice of the solvent/non solvent pair [18,19]. The morphology of the membranes was investigated by SEM. Mechanical properties, hydrophilicity and in vitro degradation rate of polymer and nanocomposite membranes were evaluated. Furthermore, we studied the biocompatibility of the new materials employing as cellular model bone marrow mesenchymal stromal cells (MSC), that are multipotent being able to differentiate into a variety of cell phenotypes including osteoblasts, and are involved in the normal remodeling and reparative mechanisms of bone [20,21]. In particular, we analyzed the adhesion, proliferation and osteogenic capacity of MSC plated on the various membranes.

2. Experimental

2.1. Materials

Polycaprolactone (PCL, CAPA 6503, molar mass 50–80 kDa, (η_{inh} 1.07 dl/g; crystallinity degree 54.8%) was purchased from Solvay (Belgium). Maleic anhydride (MA) and benzoyl peroxide (BPO) were obtained from Fluka. Glycidyl methacrylate (GMA) and N-(dimethylamino)ethylacrylate (DMAEA) were supplied by Aldrich Chemicals. All chemicals were of the highest grade commercially available. All solvents were of analytical grade and used as received. Tissue culture biochemicals were from Gibco-Invitrogen (USA) and plastic ware was supplied by BD Falcon (USA).

2.2. Functionalization of PCL

PCL modified by insertion of anhydride groups, obtained by radical grafting of maleic anhydride and glycidyl–methacrylate as a comonomer (PCL-MAGMA), and PCL modified by insertion of N-dimethylamino-ethyl acrylate (PCL-DMAEA) were prepared in a static mixer (Rheocord Haake 9000, USA), according to previously reported procedures [22,23]. The functionalized PCLs were purified by dissolution in chloroform followed by precipitation in n-hexane. For the sake of comparison, virgin PCL as well was dissolved in chloroform and re-precipitated in n-hexane before use. PCL-MAGMA (η_{inh} 0.74 dl/g; crystallinity degree 52.3%) had an amount of grafted anhydride, determined by infrared spectroscopy [24–26], equal to 2.73 wt.% (IR diagnostic band: $\nu = 1778\ cm^{-1}$). PCL-DMAEA (η_{inh} 0.94 dl/g; crystallinity degree 48.8%) had an amount of grafted amines, determined by ^1H NMR analysis, equal to 1.3 wt.% (^1H NMR diagnostic peaks (300 MHz, $CDCl_3$, δ): 2,57 (s, 6H), 3,64 (t, 2H)) (See Supplementary data).

2.3. Synthesis of hydroxyapatite nanowhiskers

HA nanowhiskers were prepared by hydrothermal method [27]. Briefly, calcined HA powders were ground by hand and dry-mixed with potassium sulfate (Tm 1069°C) at a K_2SO_4 to HA weight ratio of 1.6. The HA weight after calcination was 12.63 g and 20.20 g of potassium sulfate were added. The mixture as a compact powder was heated to a peak temperature of 1190°C for 3.5 h. The sample was allowed to cool to room temperature within the shut off furnace. The whiskers were separated from the solidified mass by washing the mass several times with hot (~90 °C) distilled water. Washing was repeated ten times; the washed whiskers were dried in an oven at 100 °C overnight (dimensions:10–20 μm long and 250 nm–2 μm in diameter).

2.4. Membrane preparation

Microporous membranes were obtained by solvent–non solvent phase inversion methodology. The polymer was dissolved in chloroform. The solution (15 wt.%) was poured into a glass petri dish, then the dish was rapidly immersed in a bath containing a large excess (about 20:1 by volume) of hexane as non-solvent. A gradual coagulation of the polymer solution was apparent at the interface with hexane, with formation of a thin skin. After 2 h the hardened polymer membrane was recovered, washed by immersion in fresh hexane and finally dried in air at room temperature. For the nanocomposite membrane preparation, HA nanowhiskers (5 wt.% with respect to the polymer) were first predispersed by sonication in a little amount of $CHCl_3$, and the dispersion was then added to the polymer solution. The resulting mixture was kept for 30 s under vigorous stirring before pouring in the petri dish.

2.5. Inherent viscosity measurements

Inherent viscosity measurements were performed at 30 °C with a Ubbelhode viscometer, at a concentration of 0.30 g/dl in $CHCl_3$.

2.6. Scanning electron microscopy (SEM)

Scanning electron microscope (FEI Quanta 200 FEG) was used to evaluate the structure of all membranes. Lower and upper surfaces were observed as such. To investigate on the bulk microporous structure, membranes were fractured after freezing in liquid nitrogen, and the fracture surface was observed. Samples were coated with Au/Pd alloy before analysis. Micrographs were taken by using a beam intensity of 20 kV.

2.7. Water contact angles measurements

Static water contact angles were determined in order to evaluate hydrophilicity. Uniform volume drops of deionized water were dropped on a horizontal portion of the membrane. The drop shape was recorded with a high speed framing camera. Contact angle was evaluated from the drop shape by measuring the angle formed between the substrate surface and the tangent drawn from the edge of the drop. Measurements were performed after a static time of 30 s.

2.8. Image analysis

Image analysis of the pores was performed using Image J software. The SEM micrographs of the fracture surfaces were digitalized and mathematically manipulated for the analysis. Pores of fairly circular shape were clearly visible in all the micrographs. For each analysis, at least 10 pores were considered. The average diameter of the pores with standard deviation was measured.

2.9. Mechanical properties

Tensile tests were carried out on nanocomposite membranes at room temperature by ISTRON 4444 instrument. Samples for tensile measurements (3 × 1 cm) were cut using a dumbbell cutter. Tensile mechanical tests were run at a crosshead speed rate of 5 mm min^{-1} and each sample was loaded to failure. Each sample was analyzed in triplicate and Young's modulus (E, MPa), ultimate stress (σ_f, MPa), ultimate strain (ε_f, %) and yield strain (ε_y, %) were expressed as the mean value of the three measurements. E was calculated using the initial linear portion of the stress/strain curves.

2.10. Hydrolytic degradation

For hydrolytic degradation studies, the samples (≈50 mg) were introduced into small flasks filled with 3 ml of phosphate buffer solution

(PBS 0.13 M, pH 7.4). Degradation was performed at 37 °C under shaking at a rate of 100 rpm for predetermined periods of time. At each degradation time point, three samples of each membrane were withdrawn and washed with distilled water. After gentle wiping to remove the remaining adsorbed water, the samples were weighed and then dried under vacuum at 40 °C for 24 h until constant weight, then weighed again.

Water uptake and weight loss values were calculated using the following equation:

$$\text{Water uptake } (\%) = \left[\left(W_{wet}\text{-}W_{dry}\right)/W_{dry}\right] \times 100 \quad (1)$$

$$\text{Weight loss } (\%) = \left[\left(W_0\text{-}W_{dry}\right)/W_0\right] \times 100 \quad (2)$$

where W_0 represents the initial weight of the samples, W_{wet} the wet weight (after wiping), and W_{dry} the dry weight.

2.11. Gel permeation chromatography (GPC)

Number average molecular weight M_n and polydispersity (Đ) of the polymers were determined by size exclusion chromatography (SEC) using a Viscotek GPCMax autosampler system fitted with two Viscotek LT5000L Mixed Medium columns (300 × 7.8 mm) and a Viscotek VE 3580 RI detector. The mobile phase was THF at 1 ml/min flow at 30 °C. Typically, the polymer (5 mg) was dissolved in THF (1 ml) and the resulting solution was filtered through a 0.45 μm Millipore filter before injection (20 μl). M_n was expressed according to calibration using polystyrene standards.

2.12. Differential scanning calorimetry (DSC)

The thermal properties were analyzed using a differential scanning calorimeter Perkin Elmer DSC 6000 fitted with a Huber CC180 cooler. Heating/cooling rate was 10 °C min^{-1} in all the experiments. To investigate the crystallization phenomenon, the following thermal treatments were performed: samples (mg) were heated from 30° to 110 °C (I run), held at this temperature for 5 min, cooled from 110 to −70 °C (II run), then heated again from −70 to 110 °C (III run).

2.13. Preparation and characterization of mesenchymal stromal cells (MSC)

Samples of human bone marrow were harvested from healthy donors, after informed consent was provided. MSC cultures were initiated as described previously [28]. Briefly, heparinized bone marrow sample was diluted 1:5 with complete culture medium consisting of Opti-MEM containing 10% fetal calf serum (FCS), antibiotics (100 units ml^{-1} penicillin, 100 mg ml^{-1} streptomycin) and incubated at 37 °C in a 5% CO_2 humidified atmosphere. After 48 h, all non-adherent cellular elements were removed and adherent spindle-like cells appeared in 3–4 days and reached sub-confluence in 1–2 weeks. Cells were then washed with phosphate buffered saline (PBS), trypsinized and amplified. The cellular model was characterized in terms of specific surface markers: the cells were positive for markers such as CD13, CD29, CD44, CD105, and CD166, and negative for hematopoietic markers CD14, CD34, and CD45. Furthermore, the multipotency of MSC was evaluated and in particular their osteogenic capacity was assessed [20,21]. Cultures between the second and fourth passages were used in the present experiments and analyzed in terms of adhesion and vitality (by PrestoBlue test and SEM observation), as well as expression of the early marker of osteoblastic phenotype, namely alkaline phosphatase (AP).

2.14. Preparation of samples for biological tests

Samples of all the membranes were obtained in the form of discs with a diameter of 22 mm that were put in 12-well plates and sterilized with 2 ml phosphate buffer containing fungizone 1% and a graded series of antibiotic solution from 10% v/v to final 1% v/v. Finally, the complete cell culture medium was added and plates were incubated for 24 h before cell plating.

2.15. Cell adhesion and viability tests

Since the surfaces of the membranes show different morphologies, due to the phase inversion method, we tested cell adhesion on both of them. MSC were seeded on membrane samples at a density of 5×10^4 cells cm^{-2} in complete culture medium and cell vitality after 48 h and 7 days was assessed by PrestoBlue assay. This reagent is a cell permeable resazurin-based solution that, when added to cells, is modified by the reducing environment of the viable cells becoming fluorescent. Cells were washed with phosphate buffered saline (PBS) and incubated with 0.5 ml of PrestoBlue 10% solution for 10 min at 37 °C. At the end of this time, the liquid was collected and the cell layer washed once with 0.5 ml of PBS. The fluorescence of the mixture was measured at 560/590 nm fluorescence excitation/emission (Perkin Elmer LS55 Luminescence Spectrometer) and expressed as Relative Fluorescence Units (RFU).

2.16. Cell morphology

In order to directly evaluate cell morphology and adhesion onto the membranes, SEM analysis was performed on samples after four days of plating. Cell layers were rinsed three times with PBS and fixed for 1 h with glutaraldehyde 0.25% vol. The fixed layers were washed again with PBS and then dehydrated by graded ethanol solutions from 30 to 100%. Samples were mounted on stubs, coated with Au/Pd alloy and examined.

2.17. Alkaline phosphatase assay

The effects on osteogenic differentiation were assessed on the seventh day of culture by analyzing the activity of the early osteoblastic marker, namely alkaline phosphatase (AP). Once the medium was removed, the wells were rinsed with 20 mM Tris/HCl-0.5 M NaCl, pH 7.4 (TBS) and the cells were then assayed in situ by adding 0.5 ml of diethanolamine phosphate buffer pH 10.5, containing 10 mM para-nitrophenyl phosphate (PNPP) and 0.5 mM $MgCl_2$. AP activity was determined by measuring the release of para-nitrophenol (PNP) from PNPP. After 15 min at 37 °C, the reaction was stopped by adding 0.5 ml of NaOH 0.5 M. PNP levels were measured spectrophotometrically at 405 nm and expressed as nmol of PNP formed in 15 min.

2.18. Statistical analysis

All the experiments were performed in triplicate on at least three different cell preparations. Data were expressed as the mean ± standard deviation (SD) of absolute values. The means of each experimental group were compared by one-way analysis of variance (ANOVA) followed by Tukey's post hoc test. Differences at p 0.05 were considered to be statistically significant.

3. Results and discussion

3.1. Functionalization of PCL

Insertion of functional groups onto the chain backbone by radical grafting is a reliable tool to modify polymers and thus gain control over some of their characteristics of interest, including mechanical and

degradation properties. Indeed, even if it is not always possible to obtain a regular, controlled distribution and length of the grafted residues, functionalization represents an easier way to chemically modify polymers with respect to more complex synthetic routes, as copolymerization. In this work, DMAEA and a MA/GMA mixture were chosen for the functionalization of PCL (Scheme 1). DMAEA, a high reactive acrylic monomer, was grafted onto the PCL backbone by a direct radical reaction. In the case of PCL-MAGMA synthesis, instead, it was necessary to add a second monomer, namely GMA, to enhance the grafting degree of MA [29]. MA is prone to copolymerize with glycidylmethacrylate, resulting in the grafting of short GMA-co-MA copolymers, as sketched in Scheme 1. The structure of PCL-MAGMA is really more complex, due to side reactions involving anhydride and glycidyl groups of GMA, with generation of carboxylic acid. The functionalization degree in terms of anhydride rings copolymerized with GMA was determined by FTIR spectroscopy on the basis of a calibration curve (see Supplementary data), and was equal to 2.7 wt.%. In the case of PCL-DMAEA, the grafting degree was evaluated by ^{1}H NMR analysis (see Supplementary data), and a value of 1.3 wt.% was obtained. Functionalization degrees were found to be reproducible. The physicochemical properties of functionalized PCL, such as thermal, mechanical, rheological behaviors and crystallization kinetics, have been deeply investigated in the previous works [22,23], and found to be significantly influenced by the chemical insertion of polar groups.

3.2. Preparation and characterization of membranes

The microstructure and architecture of an implanted device along with surface physicochemical characteristics are known to exert profound effects on cell attachment, alignment and proliferation [30,31]. Different methodologies of preparation of the device (solution casting, foaming techniques, freeze-drying, electrospinning, and so on) lead to differences in biological responses. For example, pore size and interconnectivity determine the type of tissue in growth and vascularization [32]. Relationships between pore structure, material properties and biological response are still under investigation [33]. Implant porosity can provide pathways for tissue regeneration within or over a biological scaffold or matrix. Tissue formed when the pore size is in excess than 100 μm. On the other hand, structures based on micropores less than 50 μm have been found to allow limited tissue ingrowth, required for example for stabilization of permanent implants, and this feature is desirable also in the case of membranes for the treatment of bone defects in periodontal pockets, that have the function to act as a barrier to protect the defect site from gingival tissue invasion while promoting bone healing. In the present work, microporous membranes were obtained by solvent–non solvent phase inversion method, reported in literature also for different applications such as dialysis, microfiltration, reverse osmosis, gas separation. Membranes obtained by this technique are asymmetric, with a gradational-changed microporous structure [17,34], and the two surfaces appear very different: the lower (or "cast") surface is flat, smooth, and usually porous, while the upper surface is dense and rough, as it is in direct contact with the non-solvent and a polymer skin forms at the interface with the coagulant ("skin" layer). Nevertheless, a rapid removal of the solvent may cause the rupture of the skin, giving rise to cracks.

3.2.1. SEM analysis

Upper, lower surfaces of all membranes have been investigated by SEM. No relevant differences between polymer membranes and nanocomposite membranes were pointed out in the case of external surfaces. Micrographs of nanocomposite lower surfaces are reported in Fig. 1 a–c as example. The surfaces appeared very different, being macroporous in the case of PCL/HA, microporous for PCL-DMAEA/HA, and dense for PCL-MAGMA/HA. The different porosity is mainly attributed to different degrees of adherence of the various polymers to the glass casting surface. HA nanowhiskers are clearly visible and well dispersed. On the other hand, upper surfaces are very similar for the various PCL and appeared rough, with several cracks. The upper surface of PCL-DMAEA/HA is shown in Fig. 1d as an example.

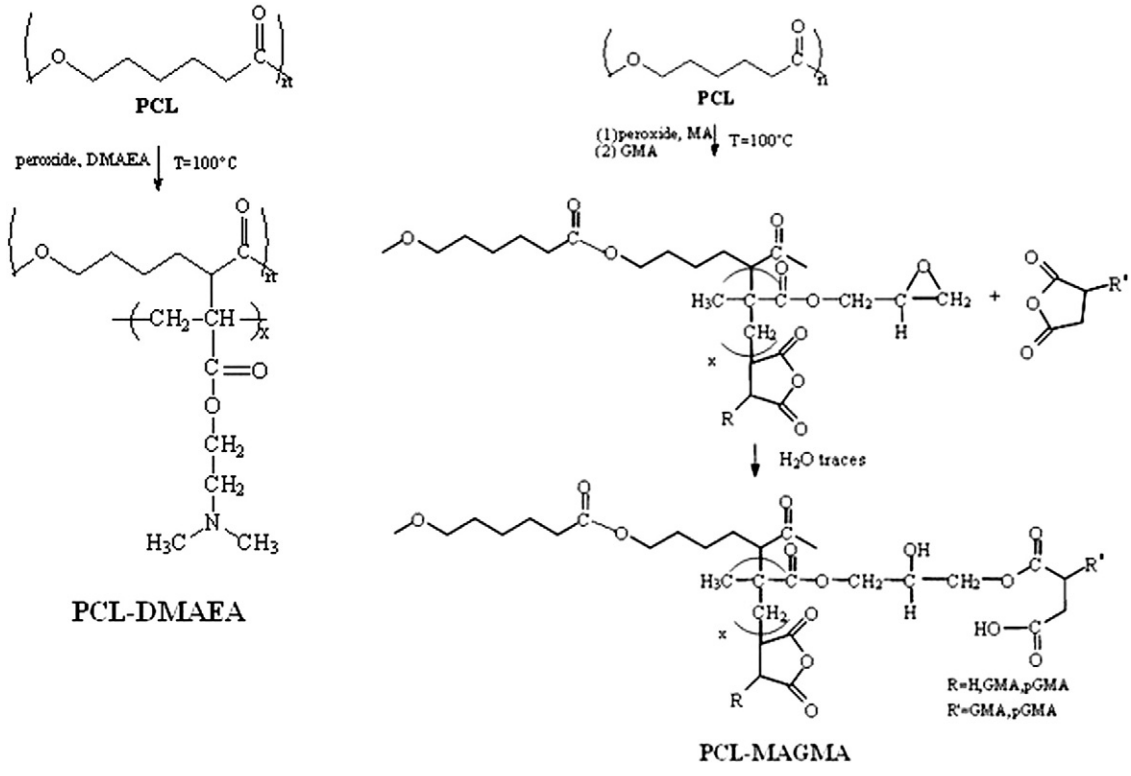

Scheme 1. Reaction schemes and structures of PCL-DMAEA and PCL-MAGMA.

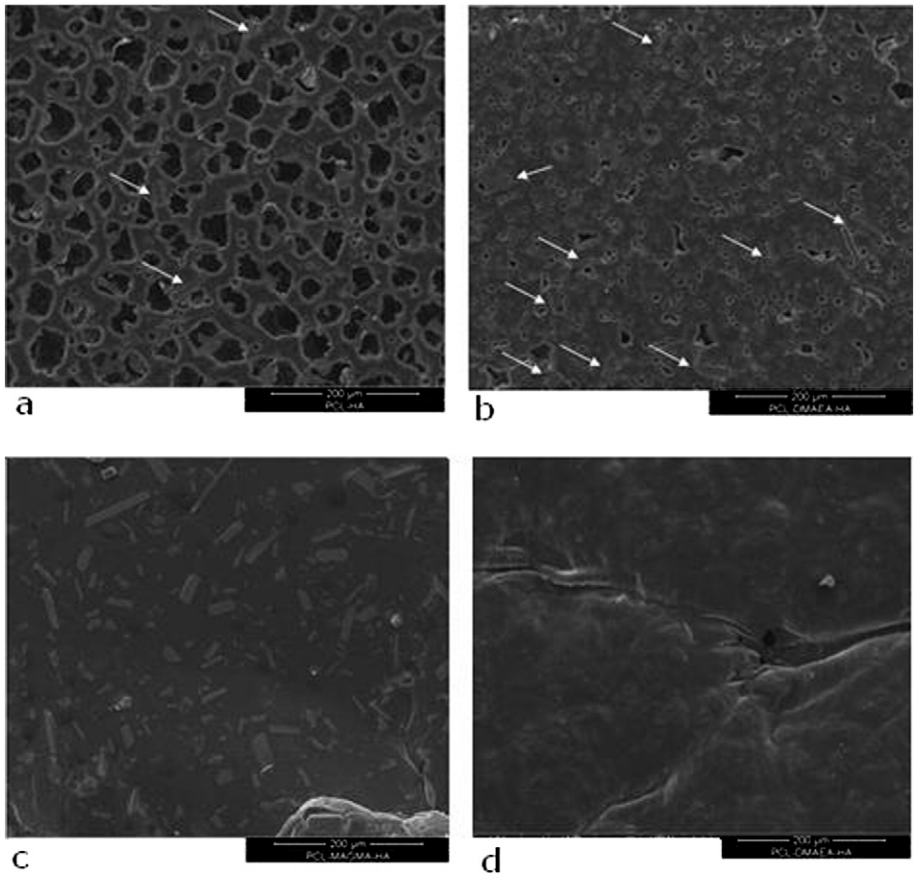

Fig. 1. SEM micrographs of lower surfaces of PCL/HA (a), PCL-DMAEA/HA (b) and PCL-MAGMA/HA (c), and upper surface of PCL-DMAEA/HA (d). (Arrows in Fig. a–b point out nanowhiskers).

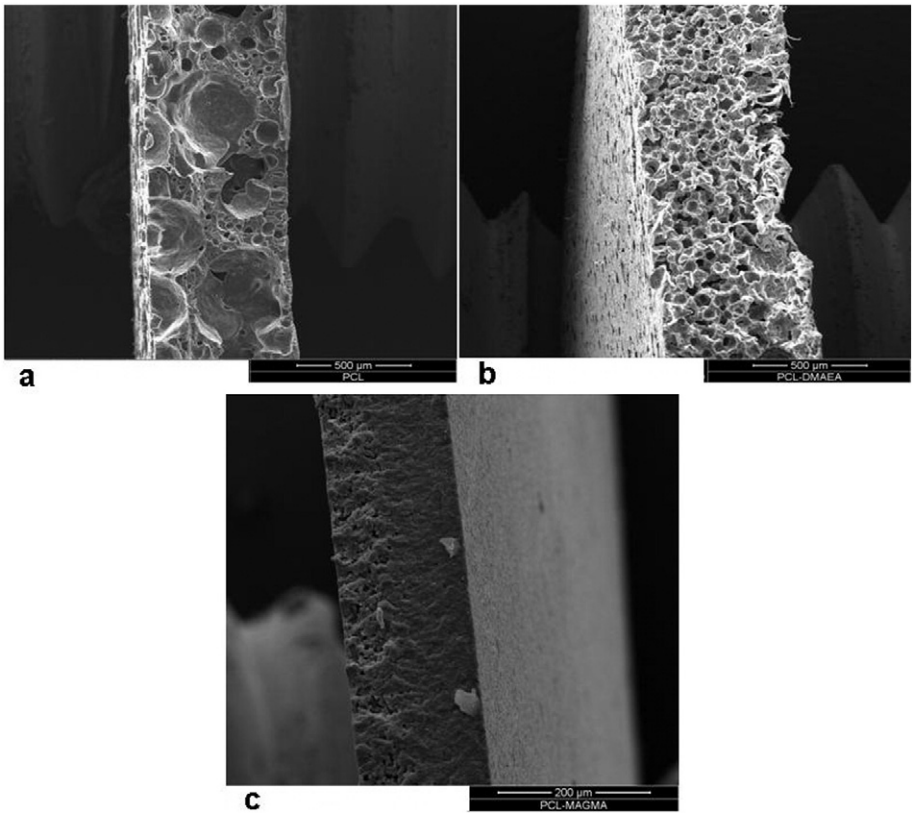

Fig. 2. SEM micrographs of fracture surfaces of PCL (a), PCL-DMAEA (b) and PCL-MAGMA (c).

Low-temperature fracture of membranes allows to expose the bulk structure. The fracture surfaces of pristine and functionalized PCL are shown in Fig. 2 a–c. A relationship between chemical structure and porosity of the membrane can be drawn. The porosity is related to coagulation time (defined as the immersion time required to reach a full polymer precipitation): the lower the time, the more porous the membrane. As a matter of fact, the porosity decreases at increasing polarity of the polymer: PCL-MAGMA coagulates as soon at is immersed in hexane, while membrane formation is slower for PCL-DMAEA and even more for PCL. Accordingly, PCL membrane has a macroporous structure (Fig. 2a), a microporous one is developed in the case of PCL-DMAEA (Fig. 2b), while PCL-MAGMA membrane is dense. (Fig. 2c).

Porosity is retained upon HA addition (Fig. 3a–c), and surprisingly a very regular microporous structure was found even in the case of PCL-MAGMA/HA. HA nanowhiskers, strongly interacting with the polymer, hamper chains association and slow down the coagulation time, giving rise to a microporous structure, in contrast with what was observed for PCL-MAGMA (Fig. 2c). HA nanowhiskers are visible at higher magnification (Fig. 4 a–c). Although many whisker pull-outs can be seen, due to the porosity of the matrix, it appears evident that the whiskers' surface looks totally polished in PCL/HA (Fig. 4a), whereas it is partially coated by the polymer in PCL-DMAEA/HA (Fig. 4b), and PCL-MAGMA/HA (Fig. 4c), indicating a better adhesion of the whiskers to the polymer.

3.2.2. Micrographs image analysis

The image analysis was performed on SEM micrographs of the fracture surface of all the membranes. The average dimension of the pores ± standard deviation (SD) is reported in Table 1.

As seen from SEM pictures, PCL, PCL/HA and PCL-DMAEA/HA show a bimodal pore distribution, with macropores of dimension ≥100 μm and micropores with dimension in the 30–70 μm range. The other samples show a more homogeneous pore distribution in the low dimension range. In particular, PCL-MAGMA membrane shows a very reduced average dimension of pores (~4 μm), not suitable for tissue regeneration, while the corresponding nanocomposite shows an average dimension falling in the range of interest (~40 μm).

3.2.3. Hydrophilicity

To assess hydrophilicity, the static water contact angle was determined (Table 2). For each membrane, contact angle measurements were carried out on both upper and lower surfaces. However, results concerning upper surfaces are not reliable, due to their roughness, and are not shown. The functionalized polymers are more hydrophilic than pristine PCL ($\theta \approx 75°$ against $\approx 97°$ for PCL), as a consequence of polar groups. Upon addition of HA, different behaviors were found for the various polymers. For PCL, the addition of HA nanowiskers led to an increase of hydrophilicity, thus resulting in PCL/HA composite with contact angles comparable to functionalized PCL-MAGMA and PCL-DMAEA. On the other hand, for the functionalized PCL nanocomposites the addition of HA has not a significant effect on contact angle values. This is attributed to the fact that, in the functionalized nanocomposites, nanowhiskers are embedded within the polymer matrix, due to the strong interactions with the grafted polar groups, and less available to water contact. However, considering the difficulty to precisely assess contact angles and that measurements are influenced by the surface porosity, these results should be considered with care as shown by the standard deviation.

3.2.4. Mechanical properties

Table 3 lists the tensile parameters of polymers and nanocomposite membranes. Overall, the porosity played a decisive role in the tensile strength and elongation at break of the membrane.

Looking at the effect of HA addition, a slight increase of E for PCL and PCL-DMAEA membranes was found, retaining the typical values ranging

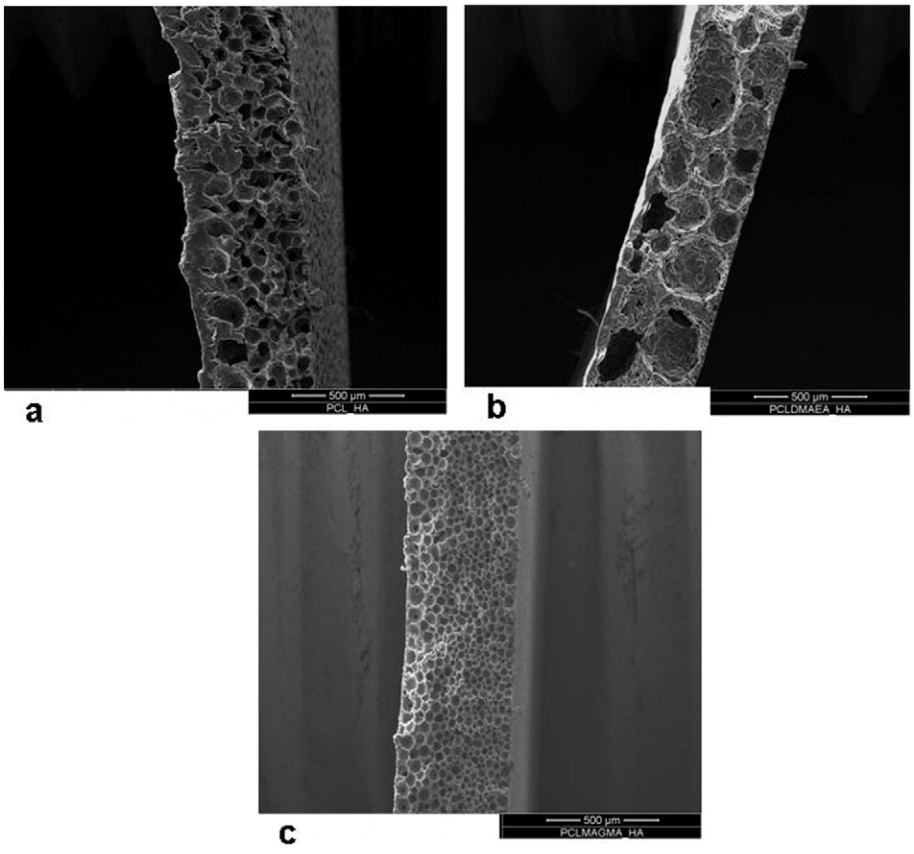

Fig. 3. SEM micrographs of fracture surfaces of PCL/HA (a), PCL-DMAEA/HA (b) and PCL-MAGMA/HA (c).

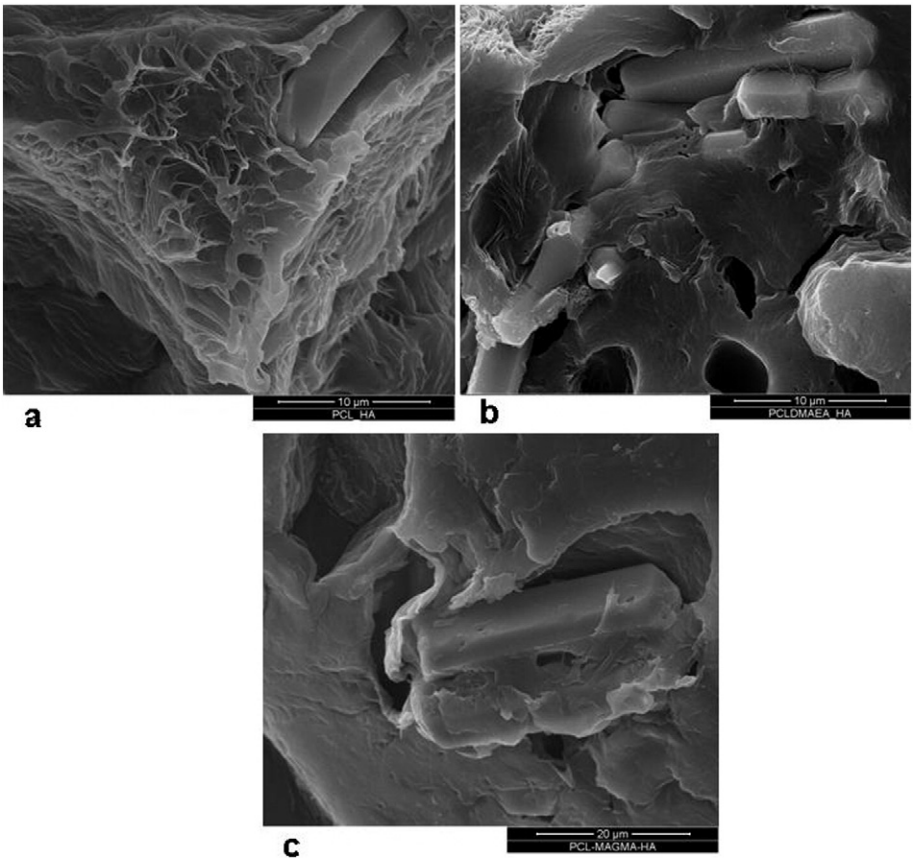

Fig. 4. SEM micrographs of HA nanowhiskers on fracture surfaces: (a) PCL/HA; (b) PCL-DMAEA/HA; (c) PCL-MAGMA/HA.

from 30 to 60 MPa. This scarce increase is in agreement with previous studies carried out on dense aliphatic polyesters/HA films showing a limited effect of the HA concentration in the range 0 to 5% [35,36]. In opposition, Young's modulus of PCL-MAGMA strongly decreased with the addition of HA, dropping from 285 MPa to 50 MPa; this drop can be attributed to the switch from dense to microporous structure, as previously discussed (Figs. 2c, 3c). As a matter of fact, such a strong decrease is not found for PCL and PCL-DMAEA matrices as they are initially porous materials (Fig. 2a, b).

Mechanical strengths (σ_f) are placed on the borderline with the reported range of interest for in vivo implantation (3–20 MPa) [17,37,38]. Three different behaviors were found upon HA addition. A poor increase was found for PCL-DMAEA/HA, as already observed for other composites [39]; PCL-MAGMA/HA ultimate stress dropped from 11.5 MPa to 2.9 MPa, due to the porosity changes, whereas non-significant change of ultimate stress was observed for PCL/HA. In opposition, ultimate strain (ε_f) values showed that for both PCL and PCL-MAGMA the addition of nanowhiskers led to extended domains or even appearance of plasticity. As discussed above, in the case of PCL-MAGMA this is mainly due to the different morphology of the membrane, although interactions between polar groups of PCL-MAGMA and HA can also have an influence by decreasing the H-bond related crystallinity of the polymer matrix [40]. In the case of PCL, morphological changes are not so pronounced, and the remarkable increase observed for PCL/HA (from 73% against up to 320%) is attributed to the decrease of crystallinity of PCL in the presence of HA nanowhiskers (see later). As shown by SEM pictures, the PCL/HA interface indicates poor adhesion between the two phases. As a consequence, HA addition tends to disorganize the PCL matrix and to decrease crystallinity without imparting strengthening, in agreement with the higher plasticity observed.

Taking into account the weight percentage of 5% HA in the nanocomposites, melting enthalpies (see Table 4) confirm the lower cristallinity of polymer phases in composites compared to pure polymers for PCL and PCL-DMAEA. The cristallinity is not affected in the case of PCL-MAGMA, which confirms that observed variations of mechanical properties can therefore be attributed only to the porosity changes.

Table 1
Pores dimension measurements taken on membrane fracture surface.

Sample	Average pore dimension [µm ± SD]
PCL	258 ± 101
	48 ± 21
PCL-DMAEA	47 ± 16
PCL-MAGMA	4 ± 1
PCL/HA	123 ± 27
	56 ± 12
PCL-DMAEA/HA	145 ± 58
	62 ± 18
PCL-MAGMA/HA	38 ± 11

Table 2
Water contact angles on membrane lower surface.

Sample	Contact angle [θ ± SD]
PCL	97 ± 6,5
PCL/HA	76 ± 6,6
PCL-DMAEA	77 ± 3,1
PCL-DMAEA/HA	70 ± 1,3
PCL-MAGMA	73 ± 6,5
PCL-MAGMA/HA	75 ± 3,8

Table 3
Mechanical parameters ± SD as obtained by tensile tests: Young's modulus (E), ultimate stress (σ_f), ultimate strain (ε_f).

Sample	E [MPa]	σ_f [MPa]	ε_f [%]
PCL	44 ± 10	3.0 ± 0.3	73 ± 12
PCL/HA	46 ± 15	3.7 ± 0.3	320 ± 88
PCL-DMAEA	33 ± 5	2.2 ± 0.5	50 ± 3
PCL-DMAEA/HA	58 ± 13	3.7 ± 0.5	42 ± 3
PCL-MAGMA	285 ± 45	11.5 ± 3.0	5 ± 1
PCL-MAGMA/HA	50 ± 8	2.9 ± 0.3	62 ± 8

3.2.5. In vitro degradation test

Degradation of polymer and nanocomposite membranes has been evaluated over a 12-month period by soaking samples in PBS at 37 °C. Thermal properties, swelling, weight loss and molecular weight decrease have been followed during the degradation. It is worth to stress that the physical integrity of samples during degradation was affected by the different functional groups. In particular, PCL-MAGMA and PCL-MAGMA/HA underwent fragmentation already after 3 months, while the other samples preserved their physical integrity during the whole degradation period. The fragmentation led to a difficult handling of PCL-MAGMA samples, in particular for what concerns the measurements of water uptake and weight loss. On the contrary, the physical state of materials during degradation did not compromise the reliability of thermal analysis.

3.2.5.1. Thermal properties. Melting temperature and melting enthalpy have been followed during degradation (Table 4). Looking at t_0 samples, it is worth to notice that the cristallinity was not affected by the addition of HA in the case of PCL-MAGMA. On the contrary, it decreased in the other PCLs. It is conceivable that polar interactions between chains in PCL-MAGMA are strong enough to be almost not affected by the addition of HA, so the crystallinity was maintained.

As can be seen in Table 4, T_m and ΔH_m increased with degradation time for all polymers and nanocomposites. This trend is a well-known behavior of aliphatic polyesters. First, T_m increase is due to the preferential degradation of the amorphous phase in the polymers and composites [40]. Secondly, crystallinity can vary during degradation and generally increases as a consequence of solvent-induced crystallization of the non-degraded polymer chains and of crystallization of the degraded chains trapped within the non-degraded bulk [41]. The variation of Tm in the range 3–8% found in the present work is in good agreement with what was previously reported for PCL sponges and films [42,43]. Regarding the evolution of ΔH_m during degradation, it is remarkable that ΔH_m variation was much higher for the functionalized PCL than for pristine PCL, as a result of the faster degradation of more hydrophilic functionalized PCL and of crystallization of the generated shorter chains. In addition, a pronounced enthalpy increase for PCL/HA (+60%) was found, against a little variation for PCL (20%), confirming the strong impact of the nanowhiskers on the PCL characteristics.

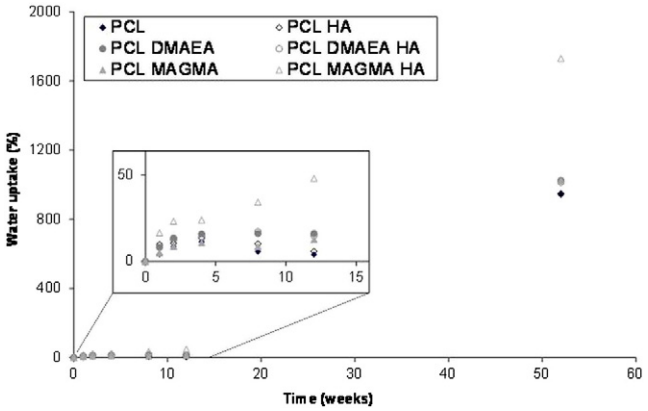

Fig. 5. Water uptake of polymers and nanocomposites as a function of degradation time (weeks).

3.2.5.2. Swelling, weight loss and molecular weight decrease. Since different hydrophilicity and porosity have been found for the various polymers and nanocomposites, different degradation behaviors as a function of their ability to hydrate and swell are expected. Fig. 5 shows the water-uptake profiles. It appears that for PCL and PCL-DMAEA the addition of 5 wt.% of HA does not influence the water-uptake which is low during the first 12 weeks for all samples. Only a little higher water-uptake was found in this initial stage for PCL-DMAEA materials compared to PCL materials. This is not surprising, as water uptake is related to the overall hydrophilicity and to bulk porosity, which helps water diffusion, and both PCL and PCL-DMAEA showed a porous structure. The hydrophilic amino groups present in PCL-DMAEA have a much higher impact on surface properties (see water contact angle measurements) than on bulk properties. After one year, all PCL and PCL-DMAEA membranes reached a final water-uptake of around 900%.

In opposition to these results, a strong influence of HA was observed for PCL-MAGMA. More in detail, whereas water-uptake of pure PCL-MAGMA was similar to the one of the other materials, water-uptake of PCL-MAGMA/HA was higher and faster, reaching 50% uptake already after 12 weeks and a final uptake two times greater than that of the other samples (1600% against about 900%).

The weight loss and molecular weight decrease over the degradation period are provided in Table 5. PCL and PCL/HA did not show any significant weight loss (<1.5%), as a result of the limited molecular weight decrease occurring in the evaluated period (about 8%). This is in agreement with previous works reporting that remarkable weight loss of PCL-based materials does not occur until the molecular weight falls to around 5000 g mol^{-1} [44]. The same behavior was observed for PCL-DMAEA and PCL-DMAEA/HA, with a negligible weight loss. However, it should be noted that the PCL-DMAEA chains have undergone a more pronounced hydrolytic degradation, with up to 15% molecular weight decrease. Finally, in opposition to what was observed for PCL and PCL-DMAEA, a significant weight loss was found for PCL-MAGMA

Table 4
Thermal properties at different degradation times.

Sample	ΔH_m [J g^{-1}]				T_m [°C]			
	t_0	3 months	12 months	ΔH_m[a] variation [%]	t_0	3 months	12 months	T_m[a] variation [%]
PCL	65	72	79	20	65	–	68	5
PCL/HA	56	51	90	60	64	67	68	6
PCL-DMAEA	68	71	96	40	63	66	67	6
PCL-DMAEA/HA	59	76	90	52	63	66	67	6
PCL-MAGMA	67	83	91	36	63	65	65	3
PCL-MAGMA/HA	65	79	92	41	59	63	64	8

[a] Percentage of variation calculated between the initial value and the value after 12 months of degradation.

Table 5
Weight loss and molecular weight decrease as a function of degradation time.

Sample	Mn/Đ [g mol^{-1}]				Weight loss [%]	
	0 month	3 months	6 months	12 months	3 months	12 months
PCL	79000/1.48	79000/1.48	76000/1.52	73000/1.53	0.5	0.9
PCL-DMAEA	77000/1.48	76000/1.49	75000/1.50	66000/1.56	0.3	0.6
PCL-MAGMA	na	na	na		5.6	11.1
PCL/HA	80000/1.48	79000/1.49	78000/1.49	74000/1.52	0.5	1.3
PCL-DMAEA/HA	77000/1.48	75000/1.50	72000/1.51	67000/1.59	0.8	–[a)]
PCL-MAGMA/HA	na	na	na		4	15.6

na: non applicable (polymers were not soluble in SEC solvent).
[a)] Not determined.

membranes, that reached around 5% weight loss already after 3 months and up to 15% after 12 months. It should be noted that this weight loss at 12 months is probably underestimated as PCL-MAGMA and PCL-MAGMA/HA underwent fragmentation already after 3 months, which made the analyses difficult. These weight loss and fragmentation are however the sign of a faster hydrolytic degradation and of an important molecular weight decrease. Unfortunately, this last point could not be confirmed by SEC analysis as a result of the poor solubility of PCL-MAGMA derivatives in THF, which proscribed the follow-up of molecular weight. This faster degradation rate may be assigned in part to the higher functionalization degree obtained with MAGMA (2.7%) compared to DMAEA (1.3%). In addition, it is also known that small amounts of amine groups act as stabilizers of polyesters by neutralizing the carboxylic acid end groups, which may explain the faster degradation of PCL-MAGMA compared to PCL-DMAEA derivatives [45]. As the optimal persistence in vivo of resorbable membranes is estimated to range from 4 weeks to one year and membranes are required to preserve their physico-mechanical characteristics during the first 4 weeks, the degradation characteristics of PCL-MAGMA/HA are of interest. Indeed, it is worth underlining that similar degradation rates have been reported in the case of PCL-PEO and PCL-PLA copolymers [41,46,47], confirming the interest of functionalization as a valid alternative to classical synthetic approaches.

3.3. Cell-biomaterial interaction study

In Fig. 6 the results of PrestoBlue assays on both membrane surfaces after 48 h MSC plating are reported. Overall both functionalized PCL showed increased cell proliferation with respect to PCL.

It has to be underlined the 2–3 fold increase in MSC adhesion onto the nanocomposites with respect to the pure polymers, attributable to the presence of hydroxyapatite, as already found for films prepared by casting [16]. Moreover, it is worth of note that the lower surfaces support colonization better than the upper ones on pure polymer membranes, whereas no relevant differences were found for nanocomposites. This trend can be explained on the basis of both the porous structure and the greater flatness and smoothness of the inferior side that was more favorable to cell attachment than the superior, more rough and dense. The surface morphology has a predominant effect in case of pure polymers, while in the nanocomposites the presence of HA on both surfaces almost cancels the gap.

Results after seven days of MSC plating (Fig. 7) substantially confirmed that the presence of hydroxyapatite was able to increase cell growth. Surprisingly, PCL showed RFU values higher than those of functionalized PCL derivatives, contrary to what was found after 48 h. Moreover, whereas for PCL, PCL-DMAEA and their nanocomposites the obtained values evidenced a significant MSC proliferation improvement compared to 48 hour values, for PCL-MAGMA and for its nanocomposite only a little growth increase was found. The explanation is based on the different porosity of the materials. In fact, the highly porous structure of PCL and PCL-DMAEA, and even more of their nanocomposites, favored cell colonization inside the pores and thus the proliferation, whereas the dense, compact structure of PCL-MAGMA and the complete absence of macropores in the related nanocomposite allowed only a little cell colonization and, consequently, a limited MSC growth. As already stated, many literature studies demonstrated that cell attachment and development are both sensitive to physicochemical properties of the substrate [30,31]. As a consequence, good cell adhesion does not necessarily induce cell spreading and migration. We can reliably assess that high porosity favors cell development (see results after seven days), while surface hydrophilicity influences mainly the initial cell adhesion (the lowest RFU value after 48 h was found for the more hydrophobic PCL).

Cell morphology and colonization on the membranes were analyzed after four days plating by scanning electron microscopy. As expected from the morphological features of membranes, the porous structure of PCL, PCL-DMAEA and their nanocomposites allowed a good spreading of cells. Fig. 8, that refers to SEM images of lower surfaces of PCL, PCL-DMAEA and corresponding nanocomposites, shows that MSC have homogeneously colonized the numerous macropores in the case of PCL-DMAEA based membranes and PCL/HA, while only sporadic cells are present on PCL (Fig. 8a). This outlook is on line with the improved

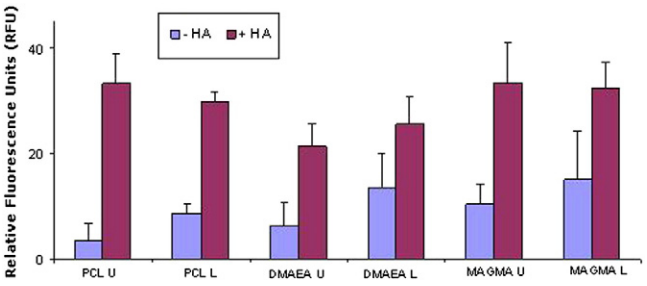

Fig. 6. PrestoBlue assay after 48 h of MSC plating onto polymers (–HA) and nanocomposites (+HA) membranes. (U = upper surface; L = lower surface).

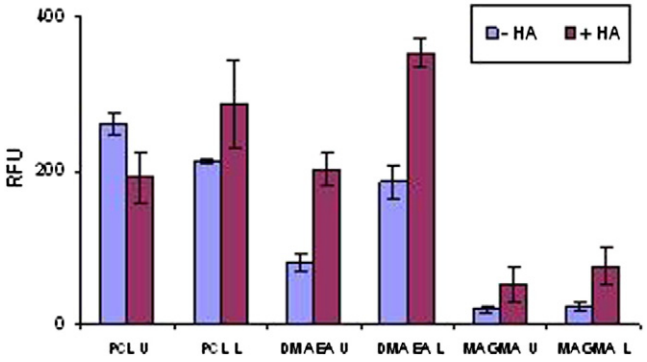

Fig. 7. PrestoBlue assay after seven days of MSC plating onto polymers (–HA) and nanocomposites (+HA) membranes. (U = upper surface; L = lower surface).

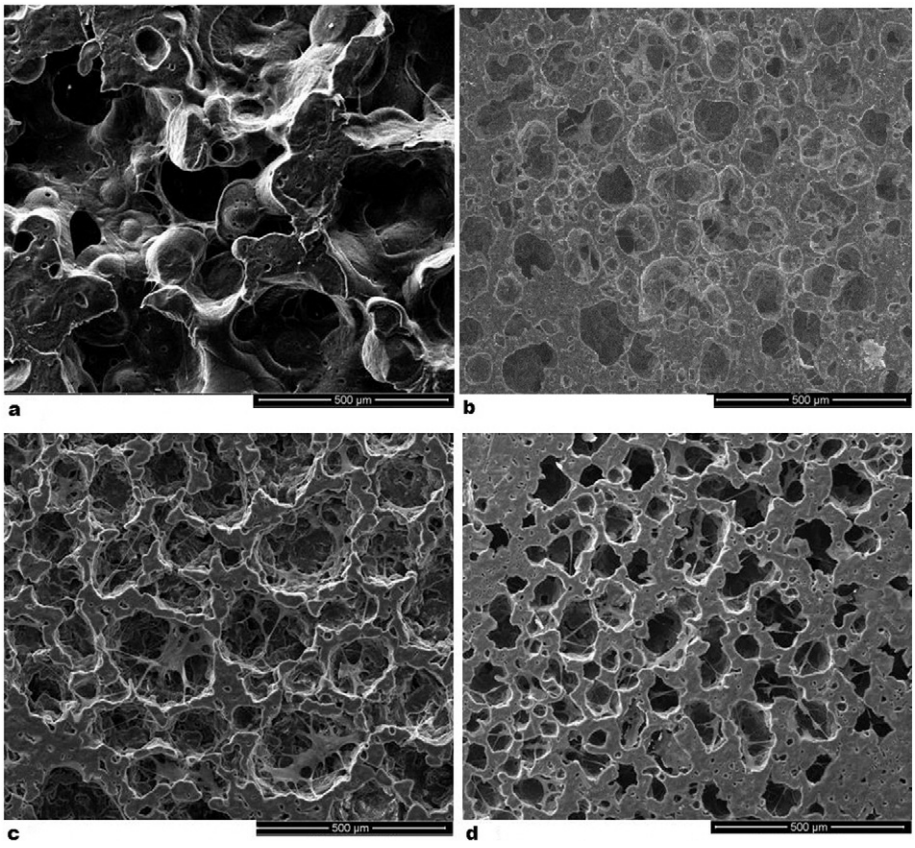

Fig. 8. SEM images of lower surfaces of PCL (a), PCL/HA (b), PCL-DMAEA (c) and PCL-DMAEA/HA (d) after four days of MSC plating.

hydrophilicity of PCL/HA and PCL derivatives with respect to the highly hydrophobic PCL. Finally, a close up of PCL-DMAEA/HA micrograph, shown in Fig. 9, stresses the presence of numerous pseudopodia that anchor the cell inside the macropore.

On the other hand, for PCL-MAGMA and its nanocomposite the denser surface prevented the widespread cell colonization, as already evidenced by PrestoBlue assay after seven days. As a consequence, micrographs of the PCL-MAGMA based membranes are not shown.

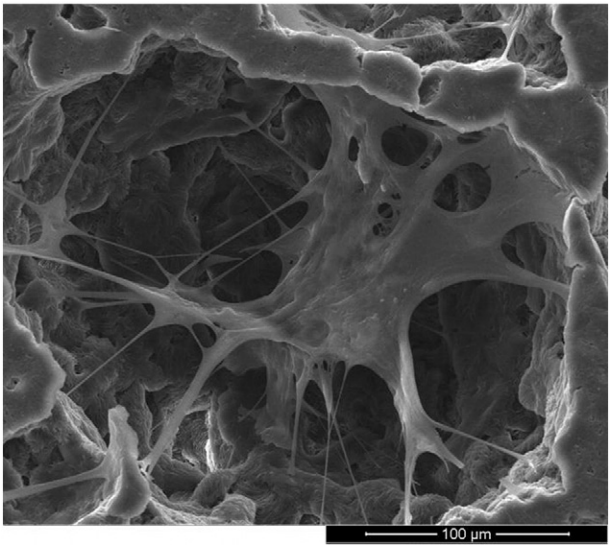

Fig. 9. SEM image of a cell anchored inside a single macropore of PCL-DMAEA/HA after four days of MSC plating.

The expression of the early biochemical marker of osteoblastic phenotype, namely alkaline phosphatase, was analyzed seven days after plating (Fig. 10). In brief, higher AP levels for PCL-DMAEA/HA and PCL-MAGMA/HA were observed with respect to the pure polymers, differently from PCL/HA. In the case of PCL, in fact, addition of hydroxyapatite did not modify substantially the levels of AP. This effect may be attributed to the widespread dispersion of nanowhiskers inside the polymer matrix in the case of functionalized PCL, that increases the availability of HA towards cell interactions.

The highest AP activity was found on cells grown on PCL-DMAEA/HA, with a not significant difference between the upper and lower surfaces. As regards PCL-MAGMA and PCL-MAGMA/HA, the low enzymatic levels were in line with the scarce colonization of cells on these materials. However, it has to be underlined that AP activity on PCL-MAGMA/HA was remarkable, if we consider the not favored spreading

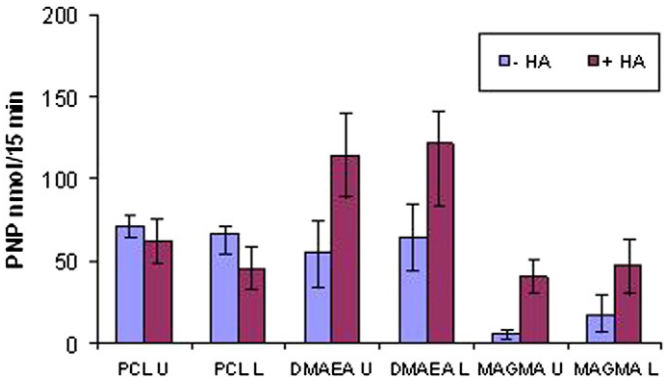

Fig. 10. Alkaline phosphatase in situ assay on MSC grown for seven days.

and, consequently, limited proliferation of cells, that in turn, could have stimulated the differentiation.

4. Conclusions

Microporous membranes for guided tissue regeneration based on PCL and on two different functionalized PCL and relative HA nanocomposites have been realized by solvent–non solvent phase inversion. The membranes have been evaluated in terms of morphology, mechanical characteristics, hydrophilicity, degradation rate and capability to provide cell attachment, proliferation and differentiation with mesenchymal stromal cells. Significant differences between the different functionalized polymers and nanocomposites were highlighted. PCL and PCL-DMAEA membranes showed a highly porous structure, whereas PCL-MAGMA membrane appeared very dense, suggesting the influence of grafted groups on the development of the porous. In opposition, nanocomposite membranes were microporous in any case. Compared to PCL, functionalized polymers showed improved surface hydrophilicity and the related nanocomposites showed homogeneous dispersion of nanowhiskers and a better HA/polymer interface. In particular, membranes based on PCL-MAGMA showed increased water uptake and degradation rate, well superior to those of PCL, so extending the field of application from long term to short-medium term supports. On the other hand, PCL-DMAEA/HA is the most promising in terms of cell adhesion, proliferation and differentiation, whereas PCL-MAGMA/HA seems to stimulate more the differentiation. Furthermore, differences in cell colonization between the two surfaces of the membranes were highlighted. This peculiarity, together with adequate pore size and mechanical strength, is of interest for the treatment of periodontal injuries, where the membrane must act as a barrier to protect the alveolar cavity from invasion of fibrous tissues, and promote bone regeneration. The nanocomposite membranes are potentially able to induce bone regeneration, particularly on the lower surface that is porous and acts as a good support for cell attachment and spreading, whereas at the same time the dense upper surface might protect the defect site from gingival epithelial cells migration.

Acknowledgments

The authors wish to thank Mrs. Cristina Del Barone and Mr. Giuseppe Narciso from laboratory “LAMEST” of IPCB-CNR for assistance in SEM analysis.

Appendix A. Supplementary data

Supplementary data to this article can be found online at http://dx.doi.org/10.1016/j.msec.2014.12.019.

References

[1] M. Vert, Aliphatic polyesters: great degradable polymers that cannot do everything, Biomacromolecules 6 (2005) 538–564.
[2] A. Sculean, D. Nikolidakis, F. Schwarz, Regeneration of periodontal tissues: combinations of barrier membranes and grafting materials—biological foundation and preclinical evidence: a systematic review, J. Clin. Periodontol. 35 (2008) 106–116.
[3] Y. Zhang, X. Zhang, B. Shi, R.J. Miron, Membranes for guided tissue and bone regeneration, Ann. Oral Maxillofac. Surg. 1 (2013) 1–10.
[4] P. Gentile, V. Chiono, C. Tonda-Turo, A.M. Ferreira, G. Ciardelli, Polymeric membranes for guided bone regeneration, Biotechnol. J. 6 (2011) 1187–1197.
[5] B. Dorj, J.E. Won, J.H. Kim, S.J. Choi, U.S. Shin, H.W. Kim, Robocasting nanocomposite scaffolds of poly(caprolactone)/hydroxyapatite incorporating modified carbon nanotubes for hard tissue reconstruction, J. Biomed. Mater. Res. A 101 (2013) 1670–1681.
[6] A. Rezaei, M.R. Mohammadi, In vitro study of hydroxyapatite/polycaprolactone (HA/PCL) nanocomposite synthesized by an in situ sol–gel process, Mater. Sci. Eng. C 33 (2013) 390–396.
[7] A. Rezaei, M.R. Mohammadi, Development of hydroxyapatite nanorods-polycaprolactone composites and scaffolds derived from a novel *in-situ* sol-gel process, Tissue Eng. Reg. Med. 9 (2012) 295–303.
[8] S. Fu, G. Guo, X. Wang, L. Zhou, T. Liu, P. Dong, F. Luo, Y. Gu, X. Shi, X. Zhao, Y. Wei, Z. Qian, Preparation and characterization of n-hydroxyapatite/PCL-pluronic-PCL nanocomposites for tissue engineering, J. Nanosci. Nanotechnol. 10 (2010) 711–718.
[9] S. Rizzi, D.J. Heath, A.G.A. Coombes, N. Bock, N.S.D. Textor, Biodegradable polymer/hydroxyapatite composites: surfaces analysis and initial attachment of human osteoblasts, J. Biomed. Mater. Res. A 55 (2001) 475–486.
[10] L. Calandrelli, B. Immirzi, M. Malinconico, I. Passaro, R. Di Pasquale, A. Oliva, Natural and synthetic hydroxyapatite filled PCL: mechanical properties and biocompatibility analysis, J. Bioact. Compat. Polym. 19 (2004) 301–313.
[11] T.J. Webster, R.W. Siegel, R. Bizios, Osteoblast adhesion on nanophase ceramics, Biomaterials 20 (1999) 1221–1227.
[12] T.J. Webster, R.W. Siegel, R. Bizios, Enhanced functions of osteoblasts on nanophase ceramics, Biomaterials 21 (2000) 1803–1810.
[13] H.H.K. Xua, D.T. Smith, C.G. Simon, Strong and bioactive composites containing nano-silica-fused whiskers for bone repair, Biomaterials 25 (2004) 4615–4626.
[14] U. Mayer, D.H. Szulczewski, K. Moeller, H. Heide, D.B. Jones, Attachment kinetics and differentiation of osteoblasts on different biomaterial surfaces, Cells Mater. 3 (1993) 129–140.
[15] W.M. Saltzmann, Cell interaction with polymers, in: R.P. Lanza, R. Langer, J. Vacanti (Eds.), Principles of Tissue Engineering, Academic Press, San Diego, 2000, pp. 221–235.
[16] M.A. Basile, G. Gomez d'Ayala, P. Laurienzo, M. Malinconico, F. Della Ragione, A. Oliva, Development of innovative biopolymers and related composites for bone tissue regeneration: study of their interaction with human osteoprogenitor cells, J. Appl. Biomater. Funct. Mater. 10 (2012) 210–214.
[17] H. Hong, J. Wei, C. Liu, Development of asymmetrical gradational-changed porous chitosan membranes for guided periodontal tissue regeneration, Compos. Part B 38 (2007) 311–316.
[18] V. Lanzetta, P. Laurienzo, G. Maglio, M. Malinconico, P. Musto, I. Schiattarella, Development and characterization of porous membranes with “sandwich-like” structure based on biocompatible, immiscible polymer blends, J. Mater. Chem. 17 (2007) 4508–4520.
[19] S. Aslan, L. Calandrelli, P. Laurienzo, M. Malinconico, C. Migliaresi, Poly(D, L-lactic acid)/(poly(ε-caprolactone) blend membranes: preparation and morphological characterisation, J. Mater. Sci. 35 (2000) 1615–1622.
[20] P. Bianco, M. Riminucci, S. Gronthos, P.J. Robey, Bone marrow stromal stem cells: nature, biology, and potential applications, Stem Cells 19 (2001) 180–192.
[21] J.R. Mauney, V. Volloch, D.L. Kaplan, Role of adult mesenchymal stem cells in bone tissue engineering applications: current status and future prospects, Tissue Eng. 11 (2005) 787–802.
[22] P. Laurienzo, M. Malinconico, G. Mattia, G. Romano, Synthesis and characterization of functionalized crosslinkable poly(ε-caprolactone) macromol, Chem. Phys. 207 (2006) 1861–1869.
[23] G. Gomez d'Ayala, E. Di Pace, P. Laurienzo, D. Pantalena, E. Somma, M.R. Nobile, Poly(ε-caprolactone) modified by functional groups: preparation and chemical physical investigation, Eur. Polym. J. 45 (2009) 3217–3229.
[24] G.M.O. Barra, J.S. Crespo, J.R. Bertolino, V. Soldi, A.T. Nunes Pires, Maleic anhydride grafting on EPDM: qualitative and quantitative determination, J. Braz. Chem. Soc. 10 (1999) 31–34.
[25] J.M. Garcia-Martinez, O. Laguna, S. Areso, E.P. Collar, FTIR quantitative characterization of chemically modified polypropylenes containing succinic grafted groups, J. Appl. Polym. Sci. 73 (1999) 2837–2847.
[26] M. Sclavons, V. Carlier, B. De Roover, P. Franquinet, J. Devaux, R.J. Legras, The anhydride content of some commercial PP-g-MA: FTIR and titration, J. Appl. Polym. Sci. 62 (1996) 1205–1210.
[27] L. Yubao, K. de Groot, J. De Wjin, C.P.A.T. Klein, S.V.D. Meer, Morphology and composition of nanograde calcium phosphate needle-like crystals formed by simple hydrothermal method, J. Mater. Sci. Mater. Med. 5 (1994) 326–331.
[28] A. Oliva, I. Passaro, A. Di Pasquale, A. Di Feo, M. Criscuolo, V. Zappia, F. Della Ragione, S. D'Amato, M. Annunziata, L. Guida, Ex vivo expansion of bone marrow stromal cells by platelet-rich plasma: a promising strategy in maxillo facial surgery, Int. J. Immunopathol. Pharmacol. 18 (2005) 47–53.
[29] X.M. Xie, N.-H. Chen, B.-H. Guo, S. Li, Study of multi-monomer chain-grafting onto polypropylene in an extruder, Polym. Int. 46 (2000) 1677–1683.
[30] C.A. Vacanti, R. Langer, B. Schloo, J.P. Vacanti, Synthetic polymers seeded with chondrocytes provide a template for new cartilage formation, Plast. Reconstr. Surg. 88 (1991) 753–759.
[31] W.S. Shalaby, S. Ikada, R. Langer, J. Williams, Polymers of biological and biomedical significance, ACS Symposium Series1994.
[32] P. Fabbri, F. Bondioli, M. Messori, C. Bartoli, D. Dinucci, F. Chiellini, Porous scaffolds of polycaprolactone reinforced with in situ generated hydroxyapatite for bone tissue engineering, J. Mater. Sci. Mater. Med. 21 (2010) 343–351.
[33] A.G.A. Coombes, S.C. Rizzi, M. Williamson, J.E. Barralet, S. Downes, W.A. Wallace, Precipitation casting of polycaprolactone for applications in tissue engineering and drug delivery, Biomaterials 25 (2004) 315–325.
[34] I. Cabasso, C.N. Tran, Polymer alloy membrane. I. Cellulose acetate-poly(bromophenylene oxide phosphonate) dense and asymmetric membranes, J. Appl. Polym. Sci. 23 (1979) 2967–2988.
[35] B. Chen, K. Sun, Mechanical and dynamic viscoelastic properties of hydroxyapatite reinforced poly (ε-caprolactone), Polym. Test. 24 (2005) 978–982.
[36] L. Lei, L. Li, L. Zhang, D. Chen, W. Tian, Structure and performance of nano-hydroxyapatite filled biodegradable poly((1,2-propanediol-sebacate)-citrate) elastomers, Polym. Degrad. Stab. 94 (2009) 1494–1502.
[37] J. Mota, N. Yu, S.C. Caridade, G.M. Luz, M.E. Gomes, R.L. Reis, J.A. Jansen, X.F. Wallboomers, J.F. Mano, Chitosan/bioactive glass nanoparticle composite membranes for periodontal regeneration, Acta Biomater. 8 (2012) 4173–4180.

[38] Y. Ikada, Tissue Engineering: Fundamentals and Applications, Academic Press, New York, 2006.
[39] C. Xianmiao, L. Yubao, Z. Yi, Z. Li, L. Jidong, W. Huanan, Properties and in vitro biological evaluation of nano-hydroxyapatite/chitosan membranes for bone guided regeneration, Mater. Sci. Eng. 29 (2009) 29–35.
[40] Z. Zhitong, S. Wenpeng, Z. Yunfei, L. Xiangde, M. Jian, Y. Yonggang, Fabrication and properties of degradable poly(aminoacid)/nano-hydroxyapatite bioactive composite, J. Appl. Polym. Sci. 125 (2012) 2502–2509.
[41] M.H. Huang, S. Li, W.-D. Hutmacher, J. Coudane, M. Vert, Degradation characteristics of poly(ε-caprolactone)-based copolymers and blends, J. Appl. Polym. Sci. 102 (2006) 1681–1687.
[42] M.N. Natu, H.C. de Sousa, H.M. Gil, Influence of polymer processing technique on long term degradation of poly(ε-caprolactone) constructs, Polym. Degrad. Stab. 98 (2013) 44–51.
[43] T. Yoshioka, F. Kamada, N. Kawazoe, T. Tateishi, G. Chen, Structural changes and biodegradation of PLLA, PCL, and PLGA sponges during in vitro incubation, Polym. Eng. Sci. 50 (2010) 1895–1903.
[44] C.G. Pitt, Y.M. Hibionada, D.M. Klimas, A. Schindler, Aliphatic polyesters. 1. The degradation of poly(ε-caprolactone) in vivo, J. Appl. Polym. Sci. 26 (1981) 3779–3787.
[45] L. Suming, S. Girod-Holland, M. Vert, Hydrolytic degradation of poly(D, L-lactic acid) in the presence of caffeine base, J. Control. Release 40 (1996) 41–53.
[46] M.H. Huang, S. Li, D.W. Hutmacher, J.T. Schantz, C.A. Vacanti, C. Braud, M. Vert, Degradation and cell culture studies on block copolymers prepared by ring opening polymerization of epsilon-caprolactone in the presence of poly(ethylene glycol), J. Biomed. Mater. Res. A 69 (2004) 417–427.
[47] M.-H. Huang, S. Li, M. Vert, Synthesis and degradation of PLA–PCL–PLA triblock copolymer prepared by successive polymerization of ε-caprolactone and DL-lactide, Polymer 45 (2004) 8675–8681.